small
NANO MICRO

Optical Materials

Size-Dependent Nonlinear Optical Properties of Atomically Thin Transition Metal Dichalcogenide Nanosheets

*Kai-Ge Zhou, Min Zhao, Meng-Jie Chang, Qiang Wang, Xin-Zhi Wu, Yinglin Song, and Hao-Li Zhang**

Size-dependent nonlinear optical properties of modification-free transition metal dichalcogenide (TMD) nanosheets are reported, including MoS_2, WS_2, and $NbSe_2$. Firstly, a gradient centrifugation method is demonstrated to separate the TMD nanosheets into different sizes. The successful size separation allows the study of size-dependent nonlinear optical properties of nanoscale TMD materials for the first time. Z-scan measurements indicate that the dispersion of MoS_2 and WS_2 nanosheets that are 50–60 nm thick leads to reverse saturable absorption (RSA), which is in contrast to the saturable absorption (SA) seen in the thicker samples. Moreover, the $NbSe_2$ nanosheets show no size-dependent effects because of their metallic nature. The mechanism behind the size-dependent nonlinear optical properties of the semiconductive TMD nanosheets is revealed by transient transmission spectra measurements.

1. Introduction

Inspired by the studies on graphene,[1] the interest in other two-dimensional (2D) nanocrystals has increased continuously.[2] The family of atomically thin, transition metal dichalcogenides (TMDs) has received considerable attention in the past few years,[2a,3] because of their unique properties, such as large surface area, high mechanical strength, high in-plane charge mobility, and weak coupling between the layers. Different from the zero-gap band structure of graphene, 2D TMD nanomaterials offer a wider range of electronic properties from insulator to metal. For instance, MoS_2 and WS_2 are semiconducting and have shown potential for use in electronic devices;[2b] whereas $NbSe_2$ is metallic and can exhibit superconductivity at low temperatures.[4] Nanosheets of TMDs have been explored for a wide range of applications as transistors,[5] photoswitches,[6] supercapacitors,[7] additives for mechanical reinforcement,[8] gas sensors,[9] and electrochemical catalysis.[10]

The fundamental physics of atomically thin TMDs is dependent not only on the type of metal and chalcogenide elements,[11] but also on the sheet size and thickness.[12] The band structure of TMDs is strongly dependent on their number of layers. For example, bulk MoS_2 is an indirect band semiconductor, but monolayer MoS_2 is a direct band material.[12] Bulk $NbSe_2$ is a typical metallic material, but monolayer $NbSe_2$ becomes a semi-metal with a low electron density near the Fermi level.[1] The size-dependent structure–property relationship provides an additional handle for the manipulation of their properties. However, very few experimental studies on size-dependent properties have been reported, partly due to the difficulty in sample preparation.

Despite numerous examples of different 2D TMD materials reported so far, the nonlinear optical (NLO) properties

Dr. K.-G. Zhou, M. Zhao, Dr. M.-J. Chang,
Prof. Q. Wang, Prof. H.-L. Zhang
State Key Laboratory of Applied Organic Chemistry
College of Chemistry and Chemical Engineering
Key Laboratory of Special Function Materials
and Structure Design
Ministry of Education
Lanzhou University
Lanzhou 730000, P.R. China
E-mail: haoli.zhang@lzu.edu.cn
X.-Z. Wu, Prof. Y. L. Song
School of Physical Science and Technology
Soochow University
Suzhou 215006, P.R. China

DOI: 10.1002/smll.201400541

of TMD nanosheets have rarely been studied.[13] In this work, we employed a *Z*-scan technique to investigate the NLO properties of three atomically thin TMDs, including two semiconductive (MoS_2 and WS_2) and one metallic ($NbSe_2$) type. We first conducted a size-separation procedure of the 2D TMD nanosheets using gradient centrifugation, and then studied the size effects on their NLO properties. Transient absorption spectra were measured to study the mechanism.

There have been a few methods developed for the preparation of single or few-layered TMD materials.[2a,14] However, some of the methods involve chemical modification of the surface of the TMD material using additives, such as, surfactants, polymers, or lithium ions, which can significantly change the intrinsic physical properties of the materials. Our group has recently developed an universal protocol to obtain stable suspensions of inorganic graphene analogues, including 2D TMDs, by liquid exfoliation in solvent mixtures.[14a] The obvious advantage of the liquid exfoliation method is that no additives are needed, so this method is less detrimental to the intrinsic physical properties of the nanomaterials. Herein, we applied this approach to produce ethanol/water dispersions of three different atomically thin TMDs: MoS_2, WS_2, and $NbSe_2$. We chose both semiconductive (MoS_2, WS_2) and metallic ($NbSe_2$) TMDs for investigation considering that NLO properties are highly dependent on the electronic band structure of the materials.

2. Results and Discussion

The exfoliation of the three materials in various ethanol/water mixtures was tested, and the optimal ethanol contents were found to be 45%, 35%, and 35% for MoS_2, WS_2, and $NbSe_2$, respectively. After a mild sonication for 8 hours, dark suspensions of MoS_2, WS_2, and $NbSe_2$ were obtained, suggesting successful exfoliation and dispersion in the corresponding ethanol/water mixtures. The original MoS_2, WS_2, and $NbSe_2$ suspensions exhibited dark green, yellow green, and pink colors, respectively. The concentrations of the suspensions were estimated from their UV-vis absorption spectra to be 0.0116, 0.137, and 0.0104 mg mL^{-1} for the MoS_2, $NbSe_2$, and WS_2 suspensions, respectively.[2a,8]

Transmission electron microscopy (TEM) measurements suggested that the as-prepared dispersions of the TMDs from liquid exfoliation contained flakes of different sizes. In order to distinguish the size effects and the intrinsic NLO response of these materials, we utilized gradient centrifugation[15] to separate the flakes with different sizes (**Scheme 1**). Briefly, a high concentration TMD suspension was firstly centrifuged at a high rotation rate. The produced supernatant was preserved for later spectroscopic characterization. Meanwhile, the sedimentation was redispersed by sonication for 5 min, and then centrifuged at a lower rate to obtain another batch of dispersed material and sedimentation. This process was repeated so that a series of suspensions that were stable in different centrifugation rate ranges were obtained. For clarification, each dispersion sample was labeled by the highest limit of its stable centrifugation region. For example, a 9000 rpm sample indicates that the dispersion was stable under a centrifugation speed of 9000 rpm or below. The centrifugation speeds used

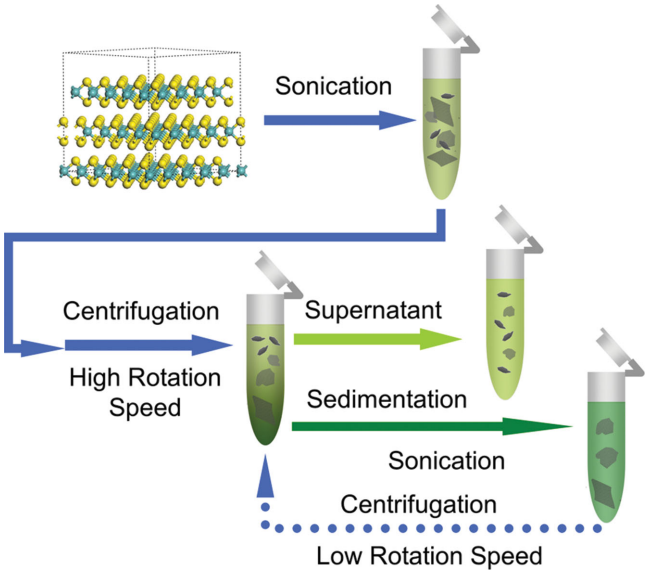

Scheme 1. The gradient centrifugation procedure to separate the TMD flakes with different sizes.

in this experiment were in the range of 3000–15 000 rpm, corresponding to a centrifugal force range from 664 g to 16 600 g.

Figure 1a shows photographs of the various suspensions of MoS_2, WS_2, and $NbSe_2$ nanosheets in ethanol/water mixtures obtained via gradient centrifugation. It can be seen that the suspensions are homogeneous with characteristic colors for different nanomaterials, a result that is consistent with our previous report.[14a] These suspensions were highly stable, and showed no precipitation after being stored for a week under ambient conditions. The colors of the TMD suspensions become lighter with increasing rotation speed. For $NbSe_2$ its suspension becames colorless at rotation speeds over 9000 rpm, implying that little material remained in the solvent. In contrast, the suspension of WS_2 can sustain much higher centrifugation speeds. Even at speeds of over 15 000 rpm, the MoS_2 and WS_2 suspensions still shows a yellow–green color. The difference in dispersibility can be attributed to the difference in size distribution of the nanomaterials, which is related to the nature of the starting materials. The better dispersibility of MoS_2 and WS_2 suggests that there are more small flakes present in their suspensions compared to that of $NbSe_2$.

Typical UV-vis spectra of the different TMD suspensions are shown in Figure 1b. The MoS_2 suspensions showed two peaks at 627 nm and 672 nm, which can be attributed to the characteristic A1 and B1 direct excitonic transitions of MoS_2 with an energy split from valence-band spin–orbital coupling.[2a] These two "spin–orbital paired" peaks indicate that the layered MoS_2 is dispersed in the solvent mixtures as the 2H-phase. The presence of nanoscale WS_2 is supported by the observation of the characteristic peak of its 2H-phase at 629 nm and 550 nm, corresponding to its "spin–orbital paired" peaks as well.[2a,16] As expected for metallic $NbSe_2$, the absorption spectrum of its suspension does not exhibit any prominent peaks. For all three TMDs, the absorbance of their suspensions decreased with increasing rotation speed.

small 2014,
DOI: 10.1002/smll.201400541

NANO MICRO small

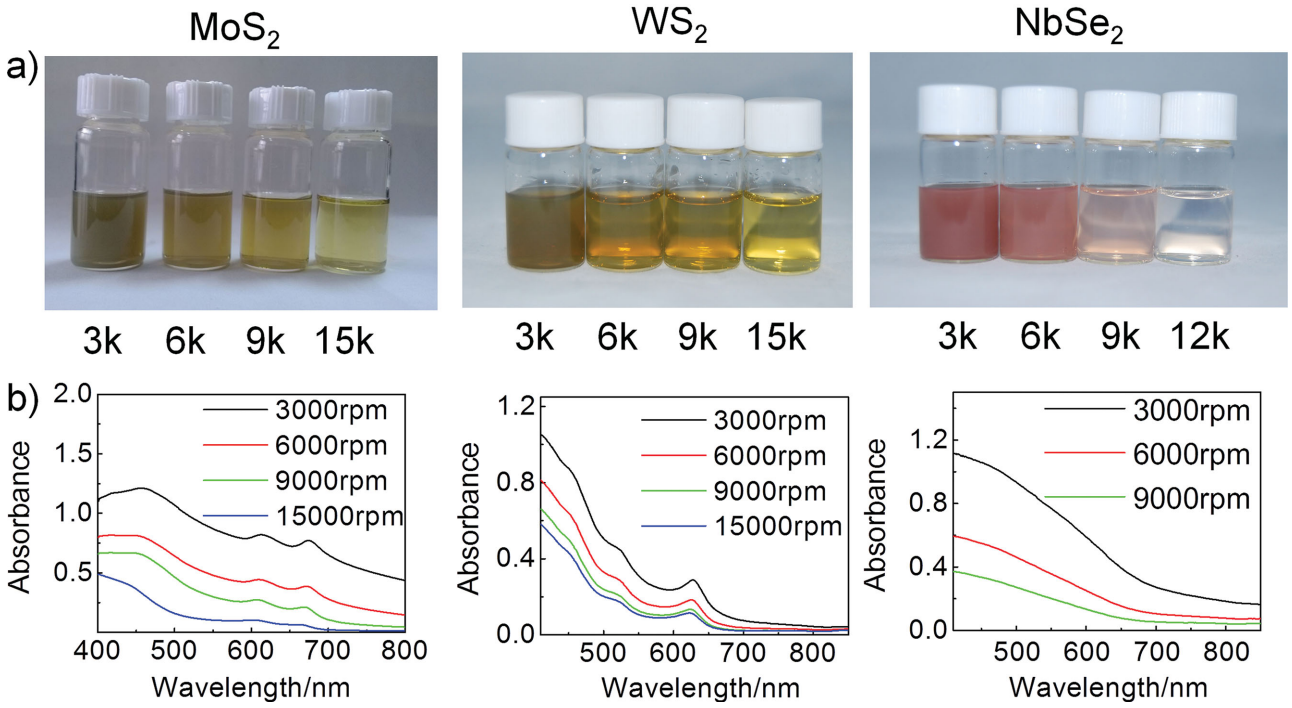

Figure 1. a) Photographs of MoS_2, WS_2, and $NbSe_2$ dispersions obtained from different centrifugation speeds; b) the corresponding UV-vis absorption spectra.

Figure 2 shows typical TEM images of the TMDs obtained at different centrifugation speeds. These TEM results suggest that all TMDs are present as 2D nanosheets in their suspensions, confirming successful exfoliation of the materials. Aggregated particles were rarely observed in these TEM images, probably because the samples have been subjected to repeated dispersion/centrifugation treatments so that large particles have been removed. The sizes of TMD nanosheets obtained in this work were mostly below 500 nm, smaller than that reported by Coleman,[15] which could be attributed to the different solvent system, starting materials, and the higher centrifugation rate used in this work. It is important to note from the TEM images that the size of TMD nanosheet shows a clear decreasing trend with increasing centrifugation speed. In the case of MoS_2, the nanosheets obtained at 3000 rpm had a maximum longitudinal length of around 500 nm, and a minimum transverse width of around 150 nm. When the rotation speed increased to 9000 rpm, the flake size decreased to around 100 nm. At the highest rotation speed of 15 000 rpm, the longitudinal length of the MoS_2 flakes reduced to around 50–60 nm. The

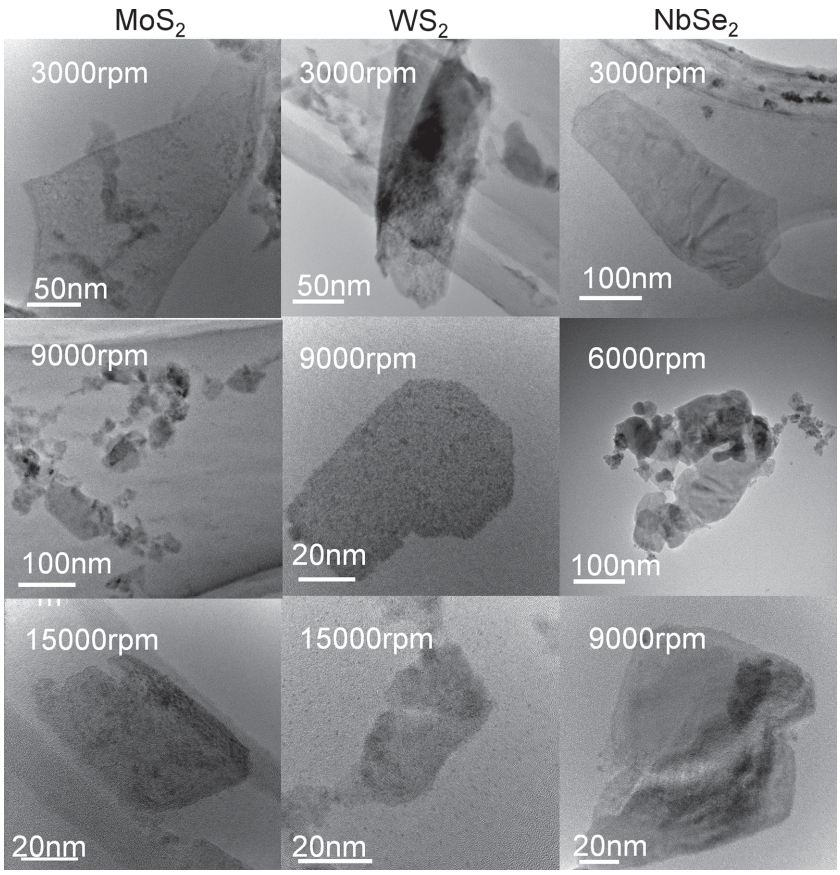

Figure 2. Representative TEM images of TMD nanoflakes obtained by gradient centrifugation. The rotation speed (rpm) at which the sample was prepared is displayed on each TEM image.

DOI: 10.1002/smll.201400541

thickness of all three MoS_2 was about 4.9 nm according to the atomic force microscopy images in Figure S2 (Supporting Information). We rarely observed any MoS_2 flakes in the dispersion obtained at rotation speeds of over 15 000 rpm. For the suspension of WS_2, the TEM results suggest that the typical flake sizes were smaller than that of MoS_2 obtained at the same rotation speeds. At a rotation speed of 3000 rpm, typical WS_2 flakes had a size of around 150 nm. TEM images indicate the presence of small WS_2 flakes in the dispersions obtained at rotation speeds of over 9000 rpm. At the highest rotation speed of 15 000 rpm, the longitudinal length of the WS_2 flakes reduced to around 50–60 nm, whereas its minimum width shrank to about 10–40 nm. High-resolution TEM images show that the flakes obtained at 15 000 rpm still preserved their hexagonal crystal lattice and the monolayers exhibited very few defects (Figure S1, Supporting Information). The thickness of all three WS_2 was found to be in the range of 4.9 to 3.8 nm (Figure S2, Supporting Information), decreasing with increasing centrifugation speed. The size of the $NbSe_2$ flakes also reduced with increasing rotation speed. The size distribution of TMDs at different rotation speeds obtained from TEM images was consistent with the hydrodynamic size distribution obtained from dynamic light scattering (DLS) measurements (Figure S3, Supporting Information). Also, the above size-distribution results at different centrifugation speeds is consistent with previous reports on graphene[17] and other TMD materials.[15]

We are interested in two types of NLO materials: saturable absorbers and optical limiters. The saturable absorbers allow the transmission of light at high optical intensities, which can be used for pulse compression, Q-switching, and mode locking.[18] The optical limiters, on the other hand, block the transmittance at high optical intensities, which may find applications in pulse shaping and laser surge protection.[19] Apart from being useful for potential applications, fundamental studies on NLO behavior can also provide insight into ultrafast charge-transfer processes in 2D nanocrystals.[20] Previous research on the NLO properties of 2D nanocrystals have only involved graphene and its derivatives.[21] Most research on pristine graphene has observed a saturated absorption in the picosecond and femtosecond region,[18] whereas a few chemically modified graphene oxides have shown optical-limiting properties.[21c] However, the size-dependence of the NLO properties has so far not been studied on 2D nanocrystals.

We applied a *Z*-scan technique to study the NLO properties of atomically thin nanosheets of TMDs in dispersion. The *Z*-scan technique is used to measure nonlinear optical properties by observing the transmittance when the sample passes through the focus.[22] The measurement system utilizes a 532-nm picosecond laser with a pumping energy of 0.5 μJ. A Q-switched and mode-locked neodymium-doped yttrium aluminum garnet (Nd:YAG) laser (Continuum model PY61) was used to generate incident light of 19 ps pulses. These pulses are short enough to exclude thermal effects on the NLO performance. More details on the set-up of the optical path can be found in the Supporting Information (Scheme S1). We used a normalized transmittance, which equals the ratio of nonlinear to linear transmittance, to evaluate the NLO properties of the different TMD samples. A normalized transmittance of 1 indicates that the material exhibits no NLO behavior. When the sample exhibits saturable absorption (SA) a normalized transmittance above 1 is expected. In contrast, a normalized transmittance below 1 indicates that the sample exhibits reverse saturable absorption (RSA). In recent *Z*-scan measurements on graphene and TMDs, both SA and RSA phenomena have been reported.[23] Herein, we applied a two-process equation[24] to fit the *Z*-scan curves:[23a]

$$\alpha = \frac{\alpha_0}{1+(I/I_S)} + \beta_{\text{eff}} I \quad (1)$$

where α_0, I, I_s, and β_{eff} are the linear absorption coefficient, incident laser intensity, saturable intensity, and effective nonlinear coefficient, respectively. The term $\alpha_0/(1+I/I_s)$ represents the SA part, which increases when I_s arises; whereas a higher β_{eff} will increase the contribution of RSA. The *Z*-scan plots of all TMD dispersions were fitted using Equation 1 and the fitting results are displayed in **Figure 3**.

It is worth mentioning that as no additives were used during sample preparation, apart from the solvents, the observed NLO phenomena shall be considered to be intrinsic of the nanoscale TMDs. Figure 3 shows that all TMD dispersions exhibit NLO behavior in the picosecond regime. For the two dispersions of MoS_2 obtained at rotation speeds of 3000 and 9000 rpm the transmittance increased sharply near the laser beam focus (zero of *Z*-position), indicating SA. Similar SA behavior of MoS_2 single-layer sheets has been observed previously in time-dependent absorbance studies.[13] The highest transmittance decreased with increasing rotation speed. In contrast, the smaller MoS_2 nanosheets (obtained at a rotation speed of over 15 000 rpm) exhibited a decreased transmittance near the zero *Z*-position. At the zero *Z*-position, the transmittance of these two samples reduced to around 95%, indicating a higher absorbance at higher laser power density, which points to RSA properties. The fitting of the *Z*-scan plots suggests that the I_s value of all MoS_2 dispersions remained around 10^{13} W m^{-2}, whereas the β_{eff} showed a dramatic difference. For the samples that are stable at rotation speeds of 3000 and 9000 rpm, the β_{eff} was around 3×10^{-15} m W^{-1}. However, the MoS_2 dispersion prepared at 15 000 rpm had a much higher β_{eff} of 5×10^{-12} m W^{-1}. Interestingly, the semiconductive WS_2 dispersions also exhibited different size-dependent NLO phenomena. The 3000 rpm WS_2 dispersion showed an increased transmittance around the zero position, indicating SA performance, which is similar to that of the large MoS_2 sheets obtained at 9000 rpm. However, smaller WS_2 nanosheets (the dispersions obtained at 9000 rpm and 15 000 rpm) exhibited a decreased transmittance near the zero *Z*-position. At the zero *Z*-position, the transmittance of these two samples was reduced to around 92%, indicating a higher absorbance at higher laser power density, pointing to RSA properties. Like MoS_2, the conversion from SA to RSA for WS_2 can also mainly be attributed to the increase in β_{eff} values. The β_{eff} of the 3000 rpm sample was 3.0×10^{-15} m W^{-1}, but it dramatically increased to $1.1–1.2 \times 10^{-11}$ m W^{-1} for the 9000 rpm and 15 000 rpm samples. Compared to the semiconductive MoS_2 and WS_2 all

small 2014,
DOI: 10.1002/smll.201400541

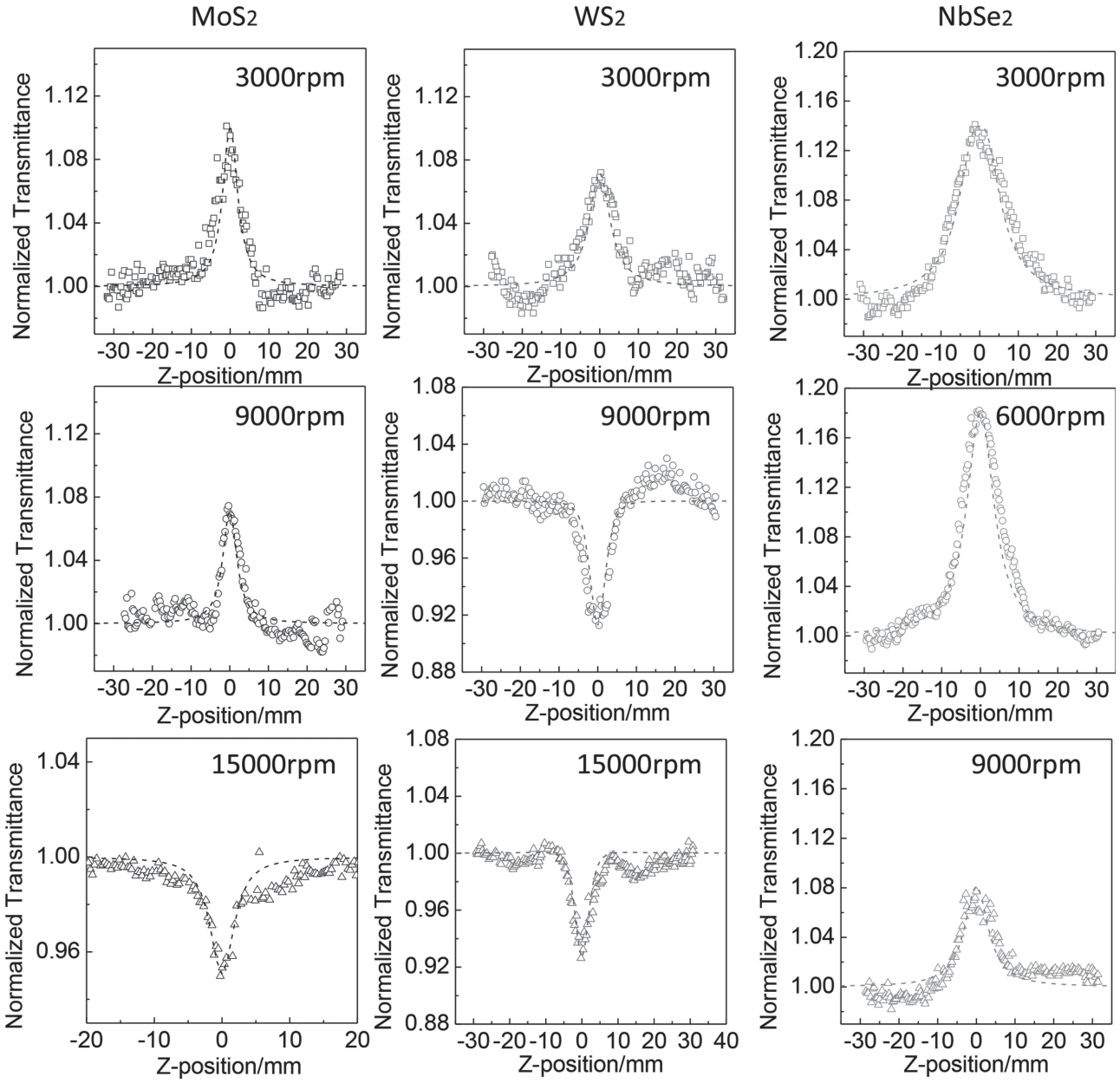

Figure 3. Open-aperture *Z*-scan measurement of the different TMD dispersions obtained by gradient centrifugation. Their transmittance was adjusted to be around 65% by diluting with original solvents.

the dispersions of metallic $NbSe_2$ showed SA phenomena. The 6000 rpm sample had a maximum transmittance of 1.136, which is close to that of few-layered graphene and graphene oxide,[21c,25] indicating a good potential for highly efficient SA devices.

The mechanism behind the NLO properties of nanomaterials is complicated as it involves many factors and in most cases is influenced by both the incident laser pulse and the intrinsic properties of the nanomaterials.[26] For nanomaterials with high absorption cross sections and a small curvature radius, the laser-induced heating could lead to solvent evaporation and micro-bubble formation around the nanomaterial. These micro-bubbles then cause thermally induced nonlinear scattering with the appearance of RSA, which has been found in the case of carbon nanotubes,[27] graphene,[21a,28] MoS_2 nanotubes[29] or nanosheets,[30] and their composites.[24] The lifetime of the micro-bubbles has been reported to be several nanoseconds.[31] In our study, such laser-heating effects can be excluded because we have used a short laser pulse of 19 ps, a pulse duration time that is much shorter than the bubble-formation time. Therefore, instead of thermal effects the intrinsic photophysics of the TMDs dominate their NLO performance in our case.

For semiconductor materials, SA phenomena are commonly observed. The main reason for the SA effect is associated with the depletion of free carriers. In the visible-light region, light absorption is mostly related to the excitation of free carriers. Under low-power incident light, the count of absorbed photons is proportional to the laser power, and the absorption coefficient is independent on the laser power.

DOI: 10.1002/smll.201400541

However, upon irradiation with a high-intensity incident laser, most of the carriers in the ground state are excited to an upper level in a very short time. Consequently, when the free carriers have been depleted, the absorption subsequently saturates with the appearance of SA properties. The mechanism of RSA is more complicated. One explanation is known as the excited-state absorption (ESA),[32] a process that has been reported on some porphyrin, phthalocyanine, and fullerene derivatives.[33] In these cases, the electrons are firstly excited from the ground state S_0 to the first singlet state S_1, and immediately pumped to S_2 within one pulse of the laser. Then, after a rapid internal conversion, S_2 falls back to S_1, and the electrons populate the first triplet state (T_1) through an intersystem crossing. As the relaxation from T_1 to S_0 is forbidden, T_1 is first excited to T_2 after which relaxation occurs. In the ESA process, the apparent nonlinear absorption has contributions from the ground, first singlet and the first triplet state absorption, therefore it becomes higher than normal absorption. On the other hand, two-photon absorption (TPA) can also induce RSA phenomena in the picosecond or femtosecond time regime. In particular, in RSA materials the second absorbed photon will further excite the metastable state before quenching. The decay of the TPA excited state will occur only after a few picoseconds, which is determined by the lifetime of the metastable states. In semiconductors, the ESA and TPA effects can exist at the same time. Boggess et al. developed a system in electronic bands (instead of molecular levels) called free-carrier absorption (FCA) to consider both ESA and TPA effects.[34] In the FCA theory, the excitation can be caused by one or two photons, in which the one-photon induced absorption is similar to the ESA mechanism.

To identify the possible mechanism behind the NLO properties in our TMD suspensions, we employed transient absorption spectroscopic measurements using a pump-probe technique with a pumping energy of 4 μJ. The pump-probe technique relies on two laser pulses: one for excitation ("pump") and the other to probe the transient spectra of the excited states ("probe") to observe the time-dependent change of the transmittance. For the sake of clarity, the transient differential transmittance was normalized as:

$$\Delta T / T_0 = (T - T_0) / T_0 \quad (2)$$

where T and T_0 are the sample transmissions with and without excitation, respectively. More details regarding the measurement conditions can be found in the Supporting Information.

Figure 4 shows the transient differential transmittance of the different TMD suspensions. We find that the signal reached a minimum instantaneously (pulse-width limited) which existed for hundreds of picoseconds, which is much longer than the duration of the laser pulse. Hence, the minimum observed here corresponds to the material properties, and are not related to laser-induced thermal effects. For the MoS_2 samples obtained at low rotation speeds the minimum was always around –0.04 without any significant change, which is consistent with similar SA phenomena

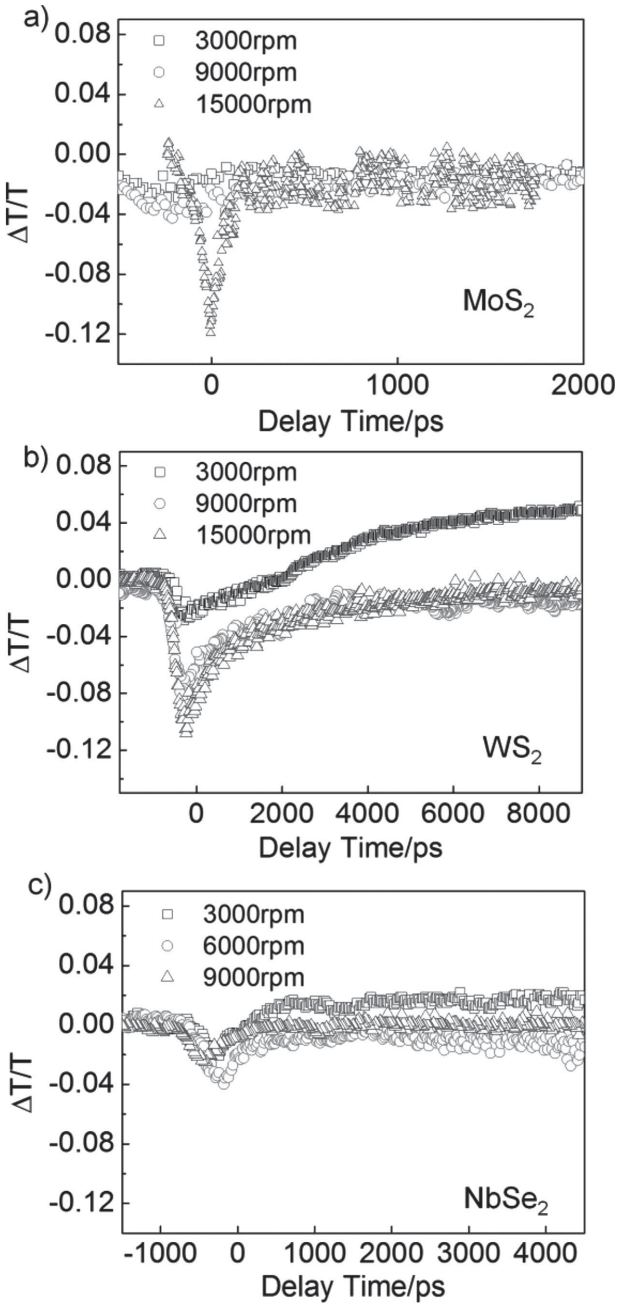

Figure 4. The transient differential transmittance of different a) MoS_2, b) WS_2, and c) $NbSe_2$ suspensions. The *y*-axes of all the plots were adjusted to the same range for clarity.

observed in the two MoS_2 dispersions obtained at 3000 rpm and 9000 rpm. However, note that the valley decreased to –0.12 in MoS_2 at 15 000 rpm, for which the *Z*-scan measurements showed RSA behavior. In contrast, the WS_2 samples obtained at the three different rotation speeds exhibited different spectra. The transient transmittance of WS_2 prepared at 3000 rpm increased continuously after its minimum of around –0.04, suggesting the depletion of carriers. But in the transmittance spectra of WS_2 obtained at 9000 rpm and above, this minimum was reduced to below –0.08, implying that the absorption cross section of the excited states was significantly reduced. Moreover, the decay time was extended to

small 2014,
DOI: 10.1002/smll.201400541

over 2000 ps without the transient differential transmittance reaching values higher than 0, implying an increased lifetime of the excited states. The transient transmittance spectra of $NbSe_2$ show a minimum around –0.04.

The transient absorption spectra provide important information regarding the excited states, and help to understand the size-dependent NLO properties of the WS_2 nanosheets. As shown above, the semiconductive MoS_2 and WS_2 flakes with sizes over 100 nm exhibited SA performance, which can be attributed to the depletion of carriers when the laser fluence increased. For small semiconductive TMD flakes, their RSA behavior indicates a more complicated mechanism. As thermal-induced scattering has been excluded, we mainly consider the ESA and TPA mechanisms. It is known that the lifetime of TPA is normally very short, for instance for graphene oxide it is 60 ps, maximum.[21c] In contrast, the lifetime of ESA can extend to several nanoseconds. Our transient absorption spectra have indicated that the excited state lifetime of the smallest WS_2 sheets was over 2000 ps; such a long lifetime is consistent with an ESA process. In addition, the TPA process occurs when the laser energy is lower than the bandgap.[35] For semiconductive MoS_2 and WS_2, their bandgaps are lower than the energy of the exciting laser, so they have more chance to absorb the 532-nm photon upon excitation and stay in an excited state rather than in a metastable state in the gap. Therefore, the RSA phenomenon of small WS_2 nanosheets can mainly be attributed to the ESA mechanism.

Due to the broken inversion symmetry, edge defects could cause the electronic structure of extremely small nanosheets to be different from that of the larger flakes,[36] which could induce ESA properties. Recently, it has been discovered that the electronic band structure[36,37] may vary with the size of semiconductive TMDs. Owing to the spin–orbital interaction induced by the unsaturated edge states, several new localized states appeared near the Fermi-level in the gap.[36] As a consequence, these edge states can act as a "springboard" to help the electrons convert to higher levels. Recent studies have shown that the edge states do significantly enhance the nonlinear optics of TMDs.[38] With smaller sizes, the proportion of edge atoms increases and, thus, they donate more to the band structure in small semiconductive TMDs than in large ones. Due to the "springboard" effect, the absorption cross section increases before the quenching of the edge states, and, thus, RSA behavior is observed. In addition, for metallic TMDs (e.g., $NbSe_2$), which do not have an intrinsic bandgap, the edge states have no effect on the excitation process as is the case in semiconductors. As a consequence, no size-dependent NLO performance was found in metallic TMDs. An even deeper understanding to NLO properties of the atomically thin TMDs can only be developed when new experimental protocols have been developed for the synthesis of TMD nanosheets with precise control over size distribution and edge states.

3. Conclusion

We have successfully prepared high-concentration suspensions of 2D nanosheets of atomically thin TMDs through liquid exfoliation. The nanosheets of TMDs with different sizes can be separated from their dispersions by gradient centrifugation, which allows their size-dependent NLO properties to be studied by *Z*-scan technique and transient absorption spectroscopy. It was found that all the $NbSe_2$ nanosheet samples showed only SA properties. For the first time, we found that nanosheets of semiconductive TMDs, such as MoS_2 and WS_2, exhibit unique size-dependent nonlinear optical properties. The samples with sizes over 100 nm exhibited SA properties, whereas the nanosheets with sizes smaller than 50 nm exhibited strong RSA phenomena. Pump-probe experiments indicated that the SA behavior of the large nanosheets of TMDs was due to carrier depletion upon excitation; and the RSA of the small nanosheets (MoS_2 and WS_2) can be mainly attributed to ESA mechanism. Such size-dependent NLO performances indicate that the same TMD material can be used in different nonlinear optical applications simply by varying its sheet size. The results of this research provide opportunity to further understand the unique optical properties of 2D TMD materials and explore their potential applications.

4. Experimental Section

Liquid Exfoliation of Atomically Thin TMDs: The samples of atomically thin TMDs were prepared by liquid exfoliation as reported before.[14a] In a typical experiment, 300 mg powder of MoS_2, WS_2 (1–6 μm, Aladdin Reagent Inc.), or $NbSe_2$ (1–6 μm, Alfa Aesar Reagent Inc.), was added into a 250 mL flask. 100 mL ethanol/water mixture with a volume fraction (EtOH v%) of 45%, 35%, or 35%, respectively, was added as the dispersion solvent. The sealed flask was sonicated for 8 h. The dispersion was then centrifuged at 3000 rpm, which equals 1062 units of gradient, for 20 minutes to remove the aggregates. Then, gradient centrifugation[15] was applied to separate the samples into different sizes. The suspensions were firstly centrifuged at a relatively high rotation speed, and the supernatant was removed and marked as the stable suspension at the given rotation speed. The sedimentations were redispersed into the dispersion solvent again by 5 min sonication, and then centrifuged at a lower rate to obtain a dispersion of TMDs stable within a certain range of centrifugation speed.

Measurements of NLO properties: The NLO properties of our TMD materials were measured by *Z*-scan technique and pump-probe in the picosecond regimes with linearly polarized 19-ps pulses (10 Hz) at 532 nm generated from a frequency doubled Q-switched Nd:YAG laser and a mode-locked Nd:YAG laser (Continuum model PY61, 10 Hz). The sample was placed at the focus where the spot radius of the pulses was about 20 μm. The reflected and transmitted pulse energies were measured simultaneously with two energy detectors (Molectron J3S-10). The measurements were calibrated using phthalocyanine. For the measurements of TMD suspensions all sample concentrations were adjusted to have the same linear transmittance of 65% at 532 nm in 1-mm thick cells.

Supporting Information

Supporting Information is available from the Wiley Online Library or from the author.

DOI: 10.1002/smll.201400541

Acknowledgements

This work is supported by the National Basic Research Program of China (973 Program) No. 2012CB933102, the National Natural Science Foundation of China (NSFC. 21233001, 21190034, 21073079, J1103307), the Specialized Research Fund for the Doctoral Program of Higher Education (SRFDP. 20110211130001), the Fundamental Research Funds for the Central Universities, and the 111 Project.

[1] K. S. Novoselov, D. Jiang, F. Schedin, T. J. Booth, V. V. Khotkevich, S. V. Morozov, A. K. Geim, *Proc. Natl. Acad. Sci. USA* **2005**, *102*, 10 451.
[2] a) J. N. Coleman, M. Lotya, A. O'Neill, S. D. Bergin, P. J. King, U. Khan, K. Young, A. Gaucher, S. De, R. J. Smith, I. V. Shvets, S. K. Arora, G. Stanton, H.-Y. Kim, K. Lee, G. T. Kim, G. S. Duesberg, T. Hallam, J. J. Boland, J. J. Wang, J. F. Donegan, J. C. Grunlan, G. Moriarty, A. Shmeliov, R. J. Nicholls, J. M. Perkins, E. M. Grieveson, K. Theuwissen, D. W. McComb, P. D. Nellist, V. Nicolosi, *Science* **2011**, *331*, 568; b) Q. H. Wang, K. Kalantar-Zadeh, A. Kis, J. N. Coleman, M. S. Strano, *Nat. Nanotechnol.* **2012**, *7*, 699.
[3] K. F. Mak, C. Lee, J. Hone, J. Shan, T. F. Heinz, *Phys. Rev. Lett.* **2010**, *105*, 136 805.
[4] a) T. Yokoya, T. Kiss, A. Chainani, S. Shin, M. Nohara, H. Takagi, *Science* **2001**, *294*, 2518; b) Y. S. Hor, U. Welp, Y. Ito, Z. L. Xiao, U. Patel, J. F. Mitchell, W. K. Kwok, G. W. Crabtree, *Appl. Phys. Lett.* **2005**, *87*, 142 506.
[5] B. Radisavljevic, A. Radenovic, J. Brivio, V. Giacometti, A. Kis, *Nat. Nanotechnol.* **2011**, *6*, 147.
[6] a) Z. Yin, H. Li, H. Li, L. Jiang, Y. Shi, Y. Sun, G. Lu, Q. Zhang, X. Chen, H. Zhang, *ACS Nano* **2012**, *6*, 74; b) H. S. Lee, S.-W. Min, Y.-G. Chang, M. K. Park, T. Nam, H. Kim, J. H. Kim, S. Ryu, S. Im, *Nano Lett.* **2012**, *12*, 3695.
[7] J. Feng, X. Sun, C. Z. Wu, L. L. Peng, C. W. Lin, S. L. Hu, J. L. Yang, Y. Xie, *J. Am. Chem. Soc.* **2012**, *133*, 17 832.
[8] R. J. Smith, P. J. King, M. Lotya, C. Wirtz, U. Khan, S. De, A. O'Neill, G. S. Duesberg, J. C. Grunlan, G. Moriarty, J. Chen, J. Wang, A. I. Minett, V. Nicolosi, J. N. Coleman, *Adv. Mater.* **2011**, *23*, 3944.
[9] H. Li, Z. Yin, Q. He, H. Li, X. Huang, G. Lu, D. W. H. Fam, A. I. Y. Tok, Q. Zhang, H. Zhang, *Small* **2012**, *8*, 63.
[10] X. Zhong, H. Yang, S. Guo, S. Li, G. Gou, Z. Niu, Z. Dong, Y. Lei, J. Jin, R. Li, J. Ma, *J. Mater. Chem.* **2012**, *22*, 13 925.
[11] a) A. Kuc, N. Zibouche, T. Heine, *Phys. Rev. B* **2011**, *83*, 245 213; b) C. Ataca, H. Şahin, S. Ciraci, *J. Phys. Chem. C* **2012**, *116*, 8983.
[12] W. S. Yun, S. W. Han, S. C. Hong, I. G. Kim, J. D. Lee, *Phys. Rev. B* **2012**, *85*, 033 305.
[13] R. Wang, B. A. Ruzicka, N. Kumar, M. Z. Bellus, H.-Y. Chiu, H. Zhao, *Phys. Rev. B* **2012**, *86*, 045 406.
[14] a) K.-G. Zhou, N.-N. Mao, H.-X. Wang, Y. Peng, H.-L. Zhang, *Angew. Chem. Int. Ed.* **2012**, *50*, 10 839; b) X. Huang, Z. Zeng, H. Zhang, *Chem. Soc. Rev.* **2013**, *42*, 1934; c) K.-K. Liu, W. Zhang, Y.-H. Lee, Y.-C. Lin, M.-T. Chang, C.-Y. Su, C.-S. Chang, H. Li, Y. Shi, H. Zhang, C.-S. Lai, L.-J. Li, *Nano Lett.* **2012**, *12*, 1538; d) Z. Zeng, Z. Yin, X. Huang, H. Li, Q. He, G. Lu, F. Boey, H. Zhang, *Angew. Chem. Int. Ed.* **2011**, *50*, 11 093.
[15] A. O'Neill, U. Khan, J. N. Coleman, *Chem. Mater.* **2012**, *24*, 2414.
[16] W. Zhao, Z. Ghorannevis, L. Chu, M. Toh, C. Kloc, P.-H. Tan, G. Eda, *ACS Nano* **2013**, *7*, 791.
[17] U. Khan, A. O'Neill, H. Porwal, P. May, K. Nawaz, J. N. Coleman, *Carbon* **2012**, *50*, 470.
[18] Q. L. Bao, H. Zhang, Y. Wang, Z. H. Ni, Y. L. Yan, Z. X. Shen, K. P. Loh, D. Y. Tang, *Adv. Funct. Mater.* **2009**, *19*, 3077.
[19] J. Wang, Y. Chen, W. J. Blau, *J. Mater. Chem.* **2009**, *19*, 7425.
[20] a) J. M. Dawlaty, S. Shivaraman, M. Chandrashekhar, F. Rana, M. G. Spencer, *Appl. Phys. Lett.* **2008**, *92*, 042 116; b) F. Xia, T. Mueller, Y.-m. Lin, A. Valdes-Garcia, P. Avouris, *Nat. Nano* **2009**, *4*, 839.
[21] a) G.-K. Lim, Z.-L. Chen, J. Clark, R. G. S. Goh, W.-H. Ng, H.-W. Tan, R. H. Friend, P. K. H. Ho, L.-L. Chua, *Nat. Photon.* **2011**, *5*, 554; b) Y. Liu, J. Zhou, X. Zhang, Z. Liu, X. Wan, J. Tian, T. Wang, Y. Chen, *Carbon* **2009**, *47*, 3113; c) Z.-B. Liu, X. Zhao, X.-L. Zhang, X.-Q. Yan, Y.-P. Wu, Y.-S. Chen, J.-G. Tian, *J. Phys. Chem. Lett.* **2011**, *2*, 1972.
[22] R. W. Boyd, *Nonlinear optics*, Academic Press, San Diego, CA **2003**.
[23] a) Z. B. Liu, Y. Wang, X. L. Zhang, Y. F. Xu, Y. S. Chen, J. G. Tian, *Appl. Phys. Lett.* **2009**, *94*, 021 902; b) Q. Y. Ouyang, H. L. Yu, K. Zhang, Y. J. Chen, *J. Mater. Chem. C* **2014**, *2*, 6319.
[24] Z. B. Liu, Y. F. Xu, X. Y. Zhang, X. L. Zhang, Y. S. Chen, J. G. Tian, *J. Phys. Chem. B* **2009**, *113*, 9681.
[25] X. Zhao, Z. B. Liu, W. B. Yan, Y. P. Wu, X. L. Zhang, Y. S. Chen, J. G. Tian, *Appl. Phys. Lett.* **2011**, *98*.
[26] a) J. B. Jun Wang and Werner, *J. Opt. A: Pure Appl. Opt.* **2009**, *11*, 024 001; b) L. W. Tutt, T. F. Boggess, *Progr. Quantum Electron.* **1993**, *17*, 299.
[27] X. Sun, R. Q. Yu, G. Q. Xu, T. S. A. Hor, W. Ji, *Appl. Phys. Lett.* **1998**, *73*, 3632.
[28] J. Wang, Y. Hernandez, M. Lotya, J. N. Coleman, W. J. Blau, *Adv. Mater.* **2009**, *21*, 2430.
[29] K. P. Loh, H. Zhang, W. Z. Chen, W. Ji, *J. Phys. Chem. B* **2005**, *110*, 1235.
[30] K. P. Wang, J. Wang, J. T. Fan, M. Lotya, A. O'Neill, D. Fox, Y. Y. Feng, X. Y. Zhang, B. X. Jiang, Q. Z. Zhao, H. Z. Zhang, J. N. Coleman, L. Zhang, W. J. Blau, *ACS Nano* **2013**, *7*, 9260.
[31] V. Kotaidis, C. Dahmen, G. von Plessen, F. Springer, A. Plech, *J. Chem. Phys.* **2006**, *124*, 184 702.
[32] J. Wang, Y. Chen, R. Li, H. Dong, L. Zhang, M. Lotya, J. N. Coleman, W. J. Blau, *Carbon Nanotubes – Synthesis, Characterization, Applications*, InTech Europe, Rijeka, Croatia **2011**; p.397.
[33] a) Y. P. Sun, G. E. Lawson, J. E. Riggs, B. Ma, N. X. Wang, D. K. Moton, *J. Phys. Chem. A* **1998**, *102*, 5520; b) S. M. O'Flaherty, J. J. Doyle, W. J. Blau, *J. Phys. Chem. B* **2004**, *108*, 17 313.
[34] T. Boggess, K. Bohnert, K. Mansour, S. C. Moss, I. Boyd, A. Smirl, *Quantum Electronics* **1986**, *22*, 360.
[35] K. P. Wang, Y. Y. Feng, C. X. Chang, J. X. Zhan, C. W. Wang, Q. Z. Zhao, J. N. Coleman, L. Zhang, W. Blau, J. Wang, *Nanoscale* **2014**, DOI: 10.1039/C4NR02634A.
[36] Y. Zhou, P. Yang, H. Zu, F. Gao, X. Zu, *Phys. Chem. Chem. Phys.* **2013**, *15*, 10 385.
[37] a) M. V. Bollinger, K. W. Jacobsen, J. K. Nørskov, *Phys. Rev. B* **2003**, *67*, 085 410; b) H. R. Gutiérrez, N. López, A. L. Elías, A. Berkdemir, B. Wang, R. Lv, F. López-Urías, V. H. Crespi, H. Terrones, M. Terrones, *Nano Lett.* **2013**, *13*, 3447; c) Y. Li, Z. Zhou, S. Zhang, Z. Chen, *J. Am. Chem. Soc.* **2008**, *130*, 16 739.
[38] X. B. Yin, Z. L. Ye, D. A. Chenet, Y. Ye, K. O'Brien, J. C. Hone, X. Zhang, *Science* **2014**, *344*, 488.

Received: February 27, 2014
Revised: August 3, 2014
Published online:

DOI: 10.1002/smll.201400541